www.acsnano.org

Predictive Biophysical Cue Mapping for Direct Cell Reprogramming Using Combinatorial Nanoarrays

Letao Yang, Brian M. Conley, Christopher Rathnam, Hyeon-Yeol Cho, Thanapat Pongkulapa, Brandon Conklin, and Ki-Bum Lee*



Downloaded via RUTGERS UNIV on July 18, 2022 at 15:24:56 (UTC). See https://pubs.acs.org/sharingguidelines for options on how to legitimately share published articles.

Cite This: ACS Nano 2022, 16, 5577-5586



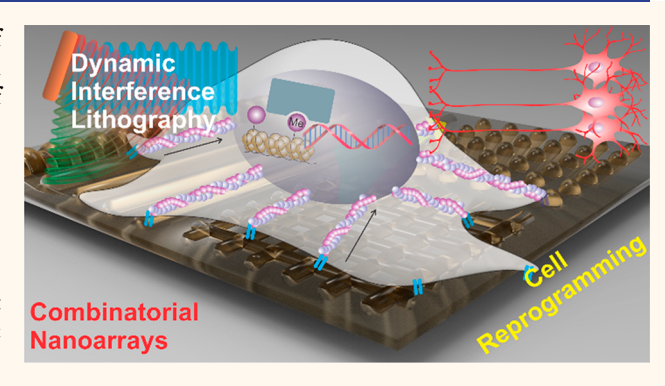
ACCESS

Metrics & More

Article Recommendations

s Supporting Information

ABSTRACT: Biophysical cues, such as nanotopographies of extracellular matrix (ECM), are key cell regulators for direct cell reprogramming. Therefore, high-throughput methods capable of systematically screening a wide range of biophysical cueregulated cell reprogramming are increasingly needed for tissue engineering and regenerative medicine. Here, we report the development of a dynamic laser interference lithography (DIL) to generate large-scale combinatorial biophysical cue (CBC) arrays with diverse micro/nanostructures at higher complexities than most current arrays. Using CBC arrays, a high-throughput cell mapping method is further demonstrated for the systematic investigation of biophysical cue-mediated direct cell reprogramming. This CBC array-based high-throughput cell screening



approach facilitates the rapid identification of unconventional hierarchical nanopatterns that induce the direct reprogramming of human fibroblasts into neurons through epigenetic modulation mechanisms. In this way, we successfully demonstrate DIL for generating highly complex CBC arrays and establish CBC array-based cell screening as a valuable strategy for systematically investigating the role of biophysical cues in cell reprogramming.

KEYWORDS: dynamic interference lithography, combinatorial nanoarrays, hierarchical nanostructures, cell reprogramming, stem cells

lthough direct cell reprogramming holds great potential for cell-based tissue engineering and regenerative medicine, realizing its full therapeutic potential requires more precise control of cell fate and a systematic understanding of the corresponding cellular responses to the surrounding microenvironments. 1-3 Direct cell reprogramming is typically regulated by dynamic interactions between multiple microenvironmental signals and alterations in the epigenetic landscape. However, the function of the cell microenvironments on epigenetic regulation of gene pathways to control cell fate or reprogramming is quite complicated, making it difficult to predict, track, and engineer.⁵ For example, there are three types of signals in cell microenvironments: soluble cues, cell-cell interactions, and insoluble/biophysical cues. Among them, insoluble/biophysical cues, such as geometry, topography, and elasticity of the extracellular matrix (ECM), have been identified as critical regulators for determining cell behaviors, including adhesion, differentiation, migration, and reprogramming. $^{6-13}$ Nevertheless, the predictive, trackable, and quantitative investigation of the functions of biophysical cues on

specific cell reprogramming processes has not been well established, which is primarily attributed to the intrinsically high heterogeneity and complexity of biophysical signaling pathways. Here is a wide range of 0D, 1D, 2D, and hierarchical micro/nano topographies and geometries have been discovered in natural (e.g., collagen fibers) and synthetic (e.g., polymer nanofibers) ECMs (Figure S1). Here slight variations within these ECM structures can cause significantly different outcomes during cell reprogramming. However, assays for systematically studying the sophisticated cellular responses to many biophysical cues, especially those associated with complex ECM structures, still require further development. Thus, there is a clear need for a more

Received: November 21, 2021 Accepted: March 15, 2022 Published: March 18, 2022





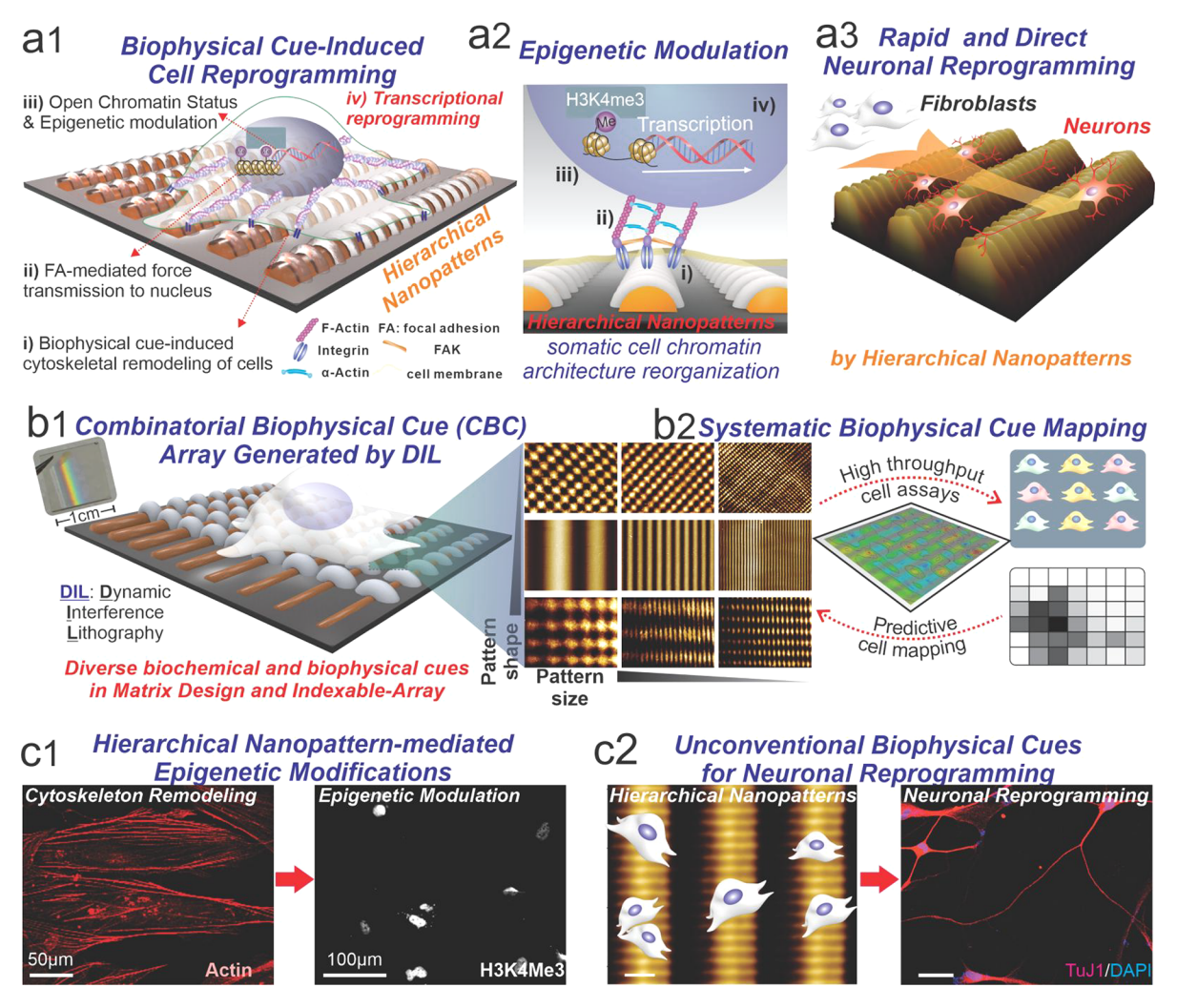


Figure 1. Predictive biophysical cue mapping and assessment approach for direct cell reprogramming using combinatorial nanoarrays. (a) Biophysical cue-induced cell reprogramming on hierarchical nanopatterns (a1) through epigenetic modulation (a2) and its applications for direct neuronal reprogramming of somatic cells (a3). The hierarchical nanopattern was identified by biophysical cue screening. (b) The generation of large-scale CBC array using a DIL approach and its application for systematic biophysical cue mapping applications. The middle panel is a representative collection of 9 AFM images (sizes of $50 \, \mu m \times 40 \, \mu m$) out of many micro/nano structures (up to millions) from one CBC array. (c) Applications of the CBC array-based cell screening for investigating nanopattern-mediated epigenetic modifications (c1) and identifying unconventional cues (e.g., hierarchical nanopatterns) for cell reprogramming (e.g., transdifferentiation of fibroblasts into neurons, c2). Scale bars: 4 and 50 μ m for the AFM (image on the left) and fluorescent images (on the right), respectively.

reliable method to investigate biophysical cues thoroughly and identify optimal biomaterial conditions for various biomedical applications; having the ability to comprehensively map cell-ECM interactions at different scales and complexities will also help us better understand the functions of biophysical signaling pathways on cell reprogramming.

To this end, we developed a dynamic interference lithography (DIL)-based method to generate combinatorial biophysical cue (CBC) arrays for predicting biophysical cue-mediated cell reprogramming (Figure 1a). Specifically, our CBC array platform contains a wide range of microscale and nanoscale topographies spanning from subhundred nanometers to tens of microns. Additionally, this large number of topographies can be readily "indexed" based on their locations on the substrate for convenient tracking of cell—ECM interactions. Unlike conventional ECM screening platforms, our CBC array can be generated in a high-throughput manner (e.g., forming thousands of ECM topographies in a few minutes) by developing a mask-free DIL technique (Figure

1b). Using this CBC array and combining it with high content cell screening, we demonstrated the mapping of biophysical cue-directed cell behaviors for facilitating the prediction of optimal nanotopographies out of numerous sophisticated ECM structures, including various combinations of micro/nano hierarchical topographies, for direct cell reprogramming (Figure 1b).

Additionally, given the considerable potential of neuronal reprogramming, we focused on identifying optimal biophysical cues to induce transdifferentiation of somatic cells (i.e., fibroblasts) into neurons in a proof-of-concept demonstration. ^{23,24} For this purpose, an unconventional hierarchical nanopattern that rapidly converts human fibroblasts into neurons was first identified by CBC array-based cell screening; then, a method was further established to generate hierarchical nanopatterns to validate this observation. Moreover, we sought to understand the underlying biophysical signaling by correlating chromatin opening, epigenetics, and the cell reprogramming outcome on the CBC array (Figure 1c). By

ACS Nano www.acsnano.org Article

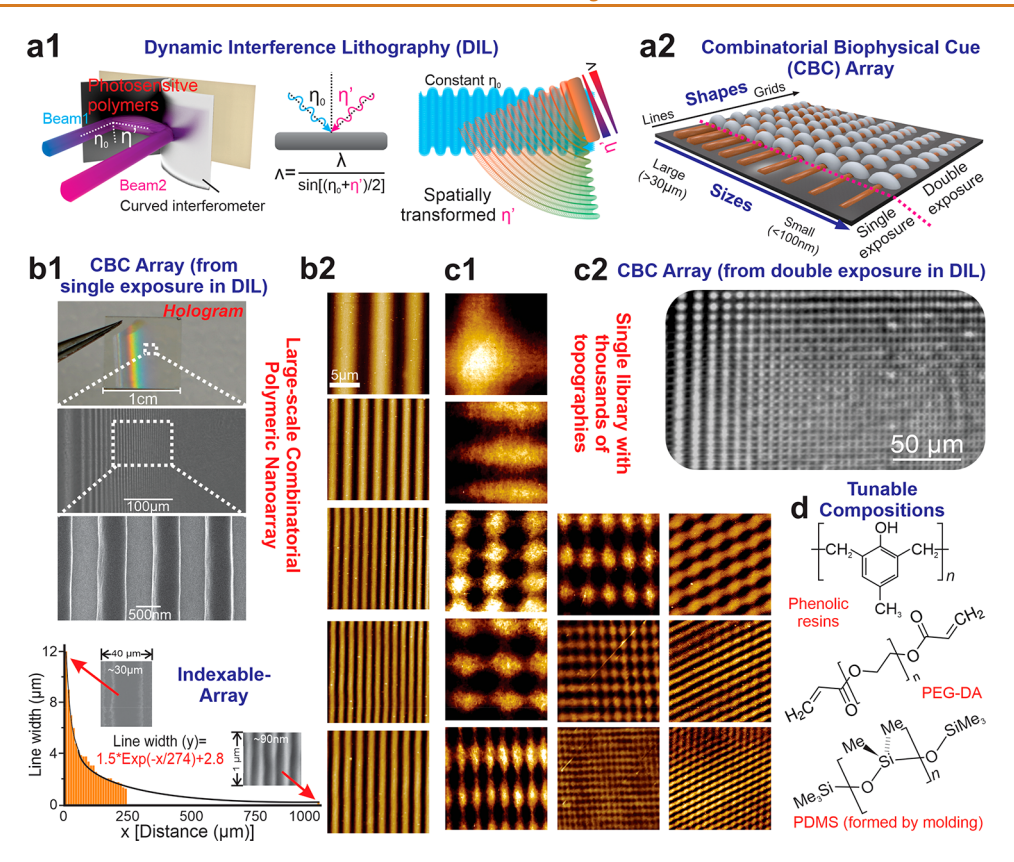


Figure 2. Combinatorial biophysical cue array generated by DIL. (a, b) Schematic diagrams showing the working principle (a1) and resulting combinatorial biophysical cue nanoarrays (a2) of DIL. (b) A representative collection of optical, SEM, HIM images (shown in b1) and AFM images (shown in b2) on different regions of the 1D line-shaped CBC arrays generated from a single laser exposure process. Graph on the bottom left is calculated from the AFM images. The x-axis indicates the distance from the boundary with largest line diameters to the nanostructure measured with the line widths or fibril diameters (y-axis). Inset SEM images indicate the general size range on the CBC array. (c) AFM images on representative regions of the more complex CBC arrays generated from double laser exposure processes. These images collectively show the diverse biophysical cues including varying dimensions, shapes, angles, and compositions of the patterns. Scale bars are identical across different images within image sets of b2 and c1. (d) Chemical structures of different photo-cross-linkable polymers/monomers [phenolic resin, polethylene glycol diacrylate (PEG-DA), and polydimethylsiloxane (PDMS, formed by molding on top of patterned phenolic resin)] for the generation of CBC arrays with varying compositions.

developing DIL and generating the CBC array-based cellular mapping platform, we aim to provide a promising alternative for current methods to systematically investigate biophysical cue-based direct cell reprogramming and advance material-mediated tissue engineering.

RESULTS AND DISCUSSION

Combinatorial Biophysical Cue Array Generated by **Dynamic Interference Lithography.** First, we developed a DIL method to generate the CBC arrays (Figure 2). Laser interference lithography (LIL), a mask-free patterning technique, has been previously applied to fabricate periodic nanostructures in a large area with high precision.^{25–27} LIL is based on Thomas Young's interference phenomenon, where the interference between two laser beams can lead to the formation of periodic standing wave patterns at their intersections.²⁸ Periodic nanostructures then can be created by exposing a photoresist layer to the standing wave, which can be described by $\Lambda = \lambda/(\sin \eta_0 + \sin \eta')$, where Λ is the period of nanostructures, λ is the wavelength of laser, and η_0 and η' are the angles between the normal to the exposed surface of beams 1 and 2, respectively. In Lloyd's mirror-based interferometer's standard setup, the interference field is static (η_0) and η' are equal and kept constant). As a result,

homogeneous photoresist nanostructures with fixed sizes and shapes are typically formed using conventional LIL (Figure S2).

We hypothesized that a nonperiodic combinatorial nanoarray with multistructural features could be fabricated by transforming one of the two beams into an infinite series of beams with various angles, leading to constant changes of η' and a dynamic progression of the interference patterns in a DIL setup (Figure 2a). First, we confirmed our hypothesis through optical simulation by identifying a convex-shaped Lloyd's mirror, which creates a series of spatially transformed laser beams with varying angles to the normal of the exposed surface (η') (Figure S3). Next, we validated the formation of the CBC array by building up an interferometer from an aluminum-coated convex mirror that reflects UV light ($\lambda = 325$ nm) following the optical simulation and confirmed that this range of topography did not induce significant variations in cell migration or proliferation within 1 day (Figures S4-S7). In nature, ECM (e.g., collagen fibrils) primarily exist in a fibrous shape with diameters ranging from subhundred nanometers to tens of microns (Figure S1). 29-31 While there have been prior attempts to generate a collection of topographies, limited success has been achieved to generate a diverse array of structures precisely. 16,26,32-36 In contrast, using DIL, a library

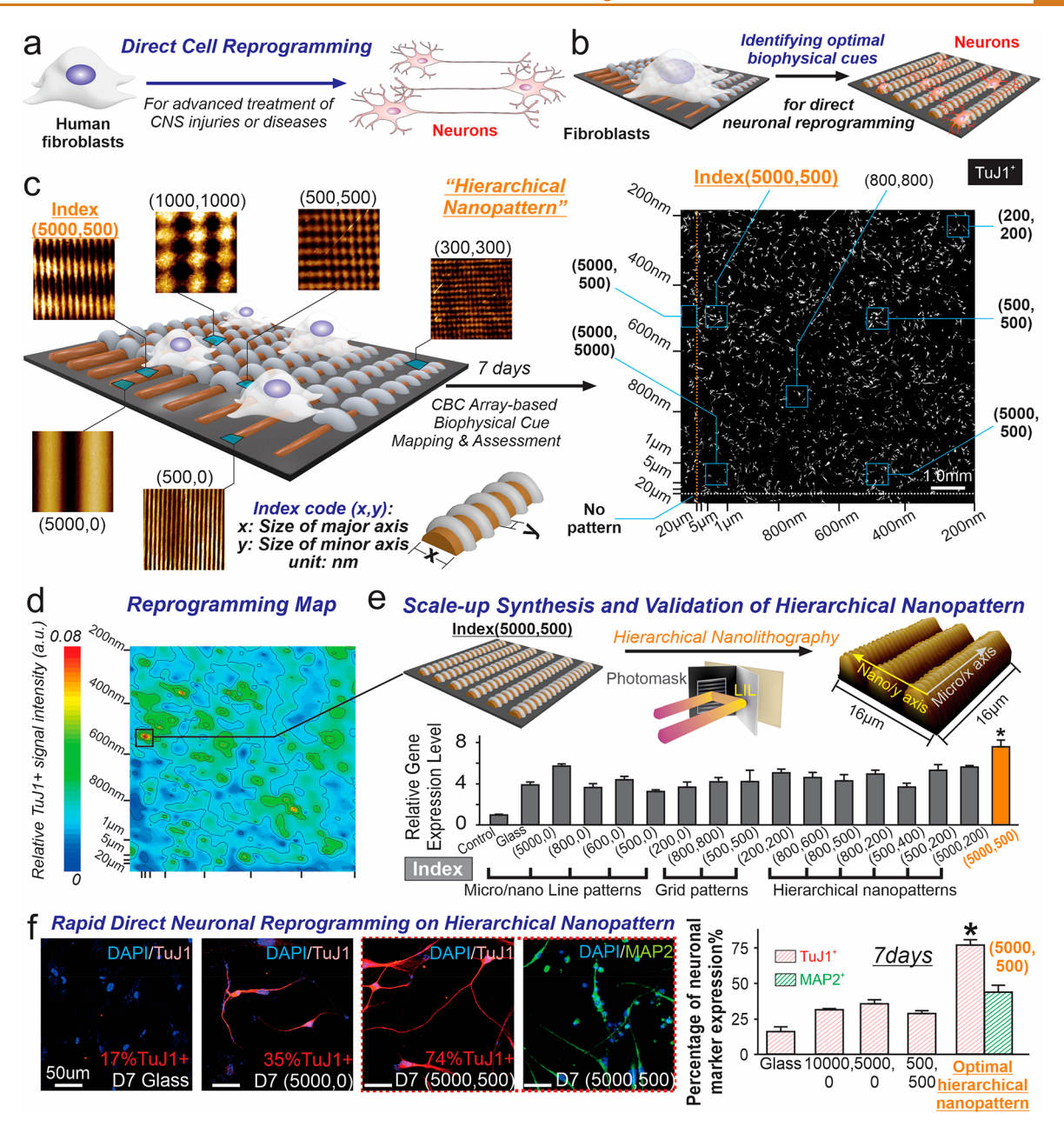


Figure 3. Assessing biophysical cue-induced cell reprogramming using CBC array-based high-throughput screening. (a, b) Schematic diagrams showing the processes of direct cell reprogramming (a) and CBC array-based high-throughput screening (b) for identifying optimal biophysical cues for direct neuronal reprogramming. (c) Indexable CBC array-based biophysical cue mapping and assessment of direct neuronal reprogramming from human fibroblasts. A hierarchical nanopattern with major and minor axis dimensions around 5000 and 500 nm [denoted as index(5000, 500), colored in blue] was identified for promoting the most efficient neuronal reprogramming. (d) Biophysical cue-based neuronal reprogramming map derived from the CBC array-based high-throughput results. (e) The scaled-up synthesis of the identified hierarchical nanopattern [index(5000, 500), scheme on the left] by developing a hierarchical nanolithography technique, which is confirmed by AFM (image on the right). (f) The scaled-up nanopattern induces the most efficient direct neuronal reprogramming based on immunostaining and qRT-PCR analysis. Scale bars in (f) 50 μ m. (e, f) n = 3 biological replicates, *P < 0.05 by one-way ANOVA with Tukey posthoc analysis.

of fiber-shaped structures spanning a wide range of sizes of natural ECM fibrils (from sub-100 nm to tens of microns) was produced based on characterizations of the scanning electron microscope (SEM) and atomic force microscope (AFM) characterizations (Figure 2b,c). In this way, we successfully validated that DIL is a reliable method to create a CBC array composed of 1D nanostructures spanning a wide range of biologically relevant sizes that are ideal for biophysical cue mapping and screening.

As the CBC array can provide many (thousands of) different nanostructures for cell studies, the characterization of the entire library and the correlation of individual nanostructures with cell behaviors becomes very challenging. We hypothesized that in our libraries, sizes (v) of varying nanostructures could be programmed and "indexed" through their positions, based on a calculation on the optical pathways, which indicates a nonlinear exponential decrease alongside the increased distance (x) (Figure 2b). This is also verified based on a

high fitting coefficient in a simulated exponential function $[\nu=1.5\times\exp(-x/274)+2.8;$ units: nm for ν and μ m for x, R^2 of 0.99] for a series of data points described by sizes (ν) of nanostructures and their locations (x defined as the distance to where the largest nanotopography feature starts), measured by nanoscale (AFM) and microscale (optical microscope) characterizations, respectively (Figure 2b,c). As cells on the library-based assays can also be identified based on the location (x), the properties (e.g., sizes) of individual ECM nanostructures could be correlated with cell behaviors at the specific location. Therefore, each nanostructure can be tracked and indexed by exponential functions for the precise, detailed, and systematic investigation of biophysical cues.

Furthermore, we sought to generate combinatorial libraries containing ECM arrays at higher complexities. In nature, ECMs can exist at higher complexities in addition to fiber-shaped 1D nanostructures.²⁹ For example, after CNS injuries (e.g., spinal cord injury), fibrous ECM can entangle each other and form grid-like patterns (Figure S1). Besides, these fibrous structures often exist at various alignment angles, from parallel to vertical to less ordered forms. Likewise, complex hierarchical ECMs can be created by the growth of nanoscale ECM on microscale fibers. The ability to recreate these diverse and complex ECM structures would allow the systematic investigation of cell–ECM interactions. 30,31 As such, we applied DIL to create libraries that include various complex ECM structures (Figure 2c). A single library that covers thousands of ECM structures, of both fibrous and grid shapes, at the nanoscale, microscale, and multiscale (hierarchical structure) can thus be created by two-step DIL with a single rotation in between, as confirmed by optical microscope, AFM and SEM (Figures S8 and S9). In addition, to mimic the different alignment angles in entangled ECM, libraries with 120° angles were synthesized as a proof-of-concept, using the two-step DIL with the same rotation angles. Besides, we can also rotate and expose the photoresist-coated substrates following an initial DIL step to generate a collection of hierarchical structures with anisotropic structural changes. In addition to structural complexities, natural ECM also spans a wide range of compositions that further lead to different mechanical properties. Therefore, we also created libraries with different compositions (Figures 2d and S9). However, the current study will solely focus on the cell-ECM interactions mediated by topographical cues alone, which plays a fundamental role in regulating cell behaviors but have not been well understood so far. In short, a versatile DIL-based nanofabrication approach was demonstrated for creating combinatorial ECM libraries spanning a wide range of structural features with structural complexities at different levels.

Assessing Biophysical Cue-Induced Cell Reprogramming Using CBC Array-Based High-Throughput Screening. We next investigated biophysical cue-mediated neuronal reprogramming of somatic cells on the CBC array generated by DIL. There has been a surge of interest in the direct neuronal reprogramming of somatic cells (e.g., fibroblasts) for clinical applications (Figure 3a). However, the low efficiency of converting somatic cells into mature neurons, which originates from the intrinsic epigenetic barriers, remains a critical hurdle for their applications in disease modeling and tissue engineering. Although several reported biophysical cues, including substrate nanotopographies, have demonstrated effects on neuronal reprogramming, a more systematic screening of

varying ECM structures would be beneficial to advance biomaterial design in neuronal reprogramming. 41-43

To this end, we first generated a neuronal reprogramming map of human fibroblasts under varying types of biophysical cues using our CBC array-based mapping method (Figure 3b,c). To do so, human fibroblasts were seeded to the CBC array followed by 3 weeks' culture in media containing minimum essential soluble factors (ISX-9, valproic acid, and CHIR9902). Afterward, cells were fixed, and their expression of early (TuJ1) and mature (MAP2) neuronal markers were visualized by immunofluorescent staining. From the large-scale $(1 \text{ cm} \times 1 \text{ cm})$ immunostaining image of cells on the CBC array, we could identify areas where cells show the brightest immunofluorescence of neuronal markers and then index the ECM structure of identified area based on their location using the exponential functions generated in the DIL study. In this case, cells in the location with estimated ECM structure 5000 nm feature in the x-axis, and 500 nm feature in the y axis, or expressed as index(5000, 500), showed the highest expression of early neuronal marker (TuJ1). Please note that this ECM structure can be directly compared to thousands of other microscale and nanoscale topographies with varying shapes (lines and grids) coexistent in a single CBC array, and thus our CBC array-based cell screening represents a highly comprehensive and less biased screening process.

Additionally, to validate our finding of index(5000, 500) as an effective inducer of neuronal reprogramming, we developed methods to scale up the synthesis of the index(5000, 500) structure in the form of a large-scale homogeneous array. Although several methods have been established for generating micro/nanohybrid topographies, it remains an ongoing challenge to fabricate large-scale (e.g., centimeter scale) homogeneous arrays of hierarchical structures in a programmable and high-throughput manner.44 We established hierarchical nanolithography by integrating a vertically aligned, microscale mask-based optical confinement system into the standard LIL setup (Figure 3d,e). By establishing this sophisticated system, we hypothesized that microscale features of the hierarchical structures could be controlled by vertically aligned microscale masks, whereas nanoscale features could be defined by the interference patterns just like a regular LIL method (Figure S10). Our hypothesis is confirmed by successfully generating our target index(5000, 500) structures using a line array photomask with 5 μ m line features vertically placed on top of the photoresist-coated substrate followed by He—Cd laser exposure in the presence of Llyod interferometer. Following etching and cleaning, an array of hierarchical structures appears, as characterized by SEM and AFM (Figure 3e). The entire process can be achieved within a few minutes, and the generated substrate can be as large as 1 cm \times 1 cm. Control nanoarrays could also be fabricated using a similar strategy, and we repeated direct cell reprogramming assay on these homogeneous arrays of index(5000, 500) as well as control conditions (Figure S11). Expression of neuronal mRNAs at day 7 was further quantified for each condition using quantitative real-time polymerase chain reaction (qRT-PCR). From the qRT-PCR assay, we verified our finding in the CBC array-based cell screening by identifying ECM (5000, 500) as the substrate condition that induces the most significant expression of TuJ1 mRNAs from fibroblasts. Moreover, we repeated the neuronal reprogramming experiments on index(5000, 500) and control substrates but characterized cells using immunofluorescent staining on a

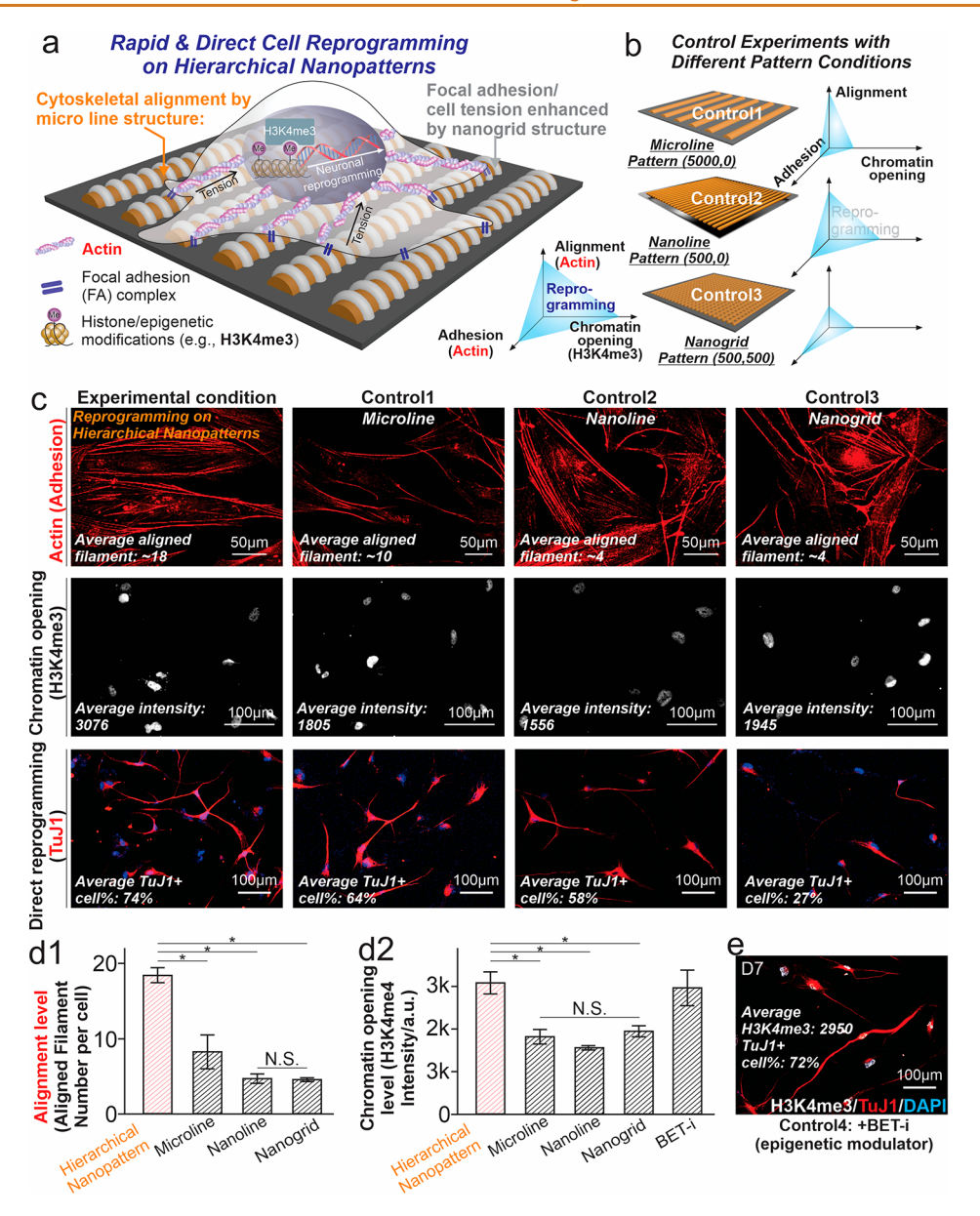


Figure 4. Demonstrating rapid cellular reprogramming via cooperative epigenetic modulation. (a, b) Proposed mechanism on the enhanced direct neuronal reprogramming on hierarchical nanopattern (a) as compared to control micro/nano patterns (b). The microline structures facilitate the alignment of cytoskeletal filaments, and nanosized features enhance the focal adhesion and tension in the aligned fibers to synergistically induce chromatin opening and overcome the epigenetic barrier in cellular reprogramming. (c, d) Immunostaining (c) and the quantification (d) on the cytoskeletal structure and chromatin opening status (H3K4me3) of fibroblasts reveal a higher number of aligned actin filaments and a stronger epigenetic modification to the DNA packaging protein Histone H3 in the hierarchical biophysical cue array compared to the control structures, which results in higher neuronal reprogramming efficiency. n = 3 biological replicates, *P < 0.05 by one-way ANOVA with Tukey posthoc analysis. (e) An immunostaining image illustrating the rapid and efficient neuronal reprogramming of fibroblast after the addition of epigenetic modulator (BET-i) on a control substrate.

mature neuronal marker (MAP2) or subtype neuronal markers (dopaminergic: TH1; excitatory: vGlut2; inhibitory: GABA) and reproduced results in the gene analysis study, thereby providing more robust evidence to support our finding in the CBC array-based cell screening (Figures S11 and S12). Notably, MAP2 positive cells differentiated from fibroblasts show clear neuron-like morphology, and they could be derived within several days without requiring any viral vectors or complex growth factor cocktails, which is much preferred for timely treatments of diseases (Figure 3f).

Demonstrating Rapid/Direct Cell Reprogramming via Cooperative Epigenetic Modulation. We were curious about how the identified ECM structure with a hierarchical nanotopography induces the most efficient neuronal reprogramming. Hierarchical structures are widely found in natural ECMs and known to affect cell differentiation; however, the systematic investigation of their effects on stem cell fate control and direct cell reprogramming has been less explored. 46–48 Our ability to precisely generate such hierarchical nanopatterns allows us to investigate the biophysical signaling associated with their effects on neuronal reprogramming. Previous literature has shown that biophysical cue-facilitated direct cell reprogramming can be achieved by altering the nuclear shape and chromatin structures or modulating transcription factor-

translocation across nuclear pores (e.g., the YAP/TAZ pathway).⁴⁹ As such, we hypothesized that our hierarchical nanopatterns could enhance direct cell reprogramming primarily through the first mechanism, as inspired by previous studies showing that microline-patterned substrates can accelerate the reprogramming of fibroblasts into human induced pluripotent stem cells (hiPSCs) through enhanced nuclear polarization and epigenetic modulation (Figure 4a,b). 50,51 More specifically, our identified hierarchical nanopattern comprises a microscale line structure (around 5000 nm in diameter) on its major axis and a nanoscale grid structure (500 nm) on top of the microlines on the minor axis. Therefore, we further hypothesized that the microline-shaped major axis could align cytoskeletal fibers (visualized by actin staining), polarize the nucleus, and open specific chromatin regions for transcriptional regulation. In parallel, nanogrids on top of the microlines, which have sizes (around 500 nm) similar to integrin clusters, could facilitate focal adhesion formation and increase the tension in the aligned cytoskeletal fibers, leading to amplification of the alignment forces induced by the microlines. 9,52 Altogether, the multiscale hierarchical nanopatterns could synergize its effects on chromatin opening and overcome the epigenetic barriers during the direct neuronal reprogramming processes (Figure 4a). Our hypothesis was directly supported by observing a significantly higher (over two-fold) density of aligned actin fibers within the fibroblasts cultured on the experimental condition [index (5000, 500)], as compared to the control substrates [line ECM structures: index(5000, 0); grid ECM structures: index(500, 500); and PR-coated glass substrates [Figures 4c,d and S12]. In addition, the better-aligned cytoskeleton of fibroblasts in our experimental condition was also correlated to an increased expression of H3K4me3, a representative epigenetic modification indicating the opening of chromatin (Figure 4c,d).⁵³ To further support this, we also added a soluble form of epigenetic modulator [bromodomain extra-terminal inhibitor (BET-i)] to fibroblasts cultured on control substrates (glass), and a significantly enhanced conversion of fibroblasts into neurons within 7 days following the addition of BET-I verified the importance of epigenetic modulation for cell reprogramming (Figure 4e). 53,54 While further genomic and transcriptomic studies would be helpful to fully elucidate the mechanism of enhanced conversion, our CBC array-based mapping platform and assessment approaches showed excellent potential for predicting and investigating biophysical cues at higher complexities in the direct cell reprogramming.

CONCLUSIONS

In summary, our work demonstrated a predictive mapping platform to investigate biophysical cues by developing a nanofabrication approach that generates combinatorial biophysical cue arrays at various complexities. Through this, we identified a hierarchical nanotopography for inducing efficient direct cell reprogramming via cytoskeletal remodeling and chromatin opening. Specifically, we presented a way to fabricate combinatorial nanoarrays. Several recent studies have synthesized combinatorial micro/nanostructures for cell applications. ^{16,33,36} Our approach allows many complex structures spanning tens of nanometers to tens of microns to be formed in a precise and indexable manner. The nanofabrication (DIL) was achieved by spatially transforming static interference fields into a series of dynamically changing interference events. The interferometric nature of our

nanofabrication method for synthesizing combinatorial nanoarrays allows incorporating different light-sensitive materials (e.g., hydrogels) and topographies for versatile biological screening applications in the future. Indeed, the combinatorial nanoarray can be applied to investigate the design and understanding of various material properties (e.g., optical, mechanical, and magnetic) and functions. Next, a predictive cell mapping platform to systematically investigate cell-ECM interactions was developed. Utilizing the CBC array, we further established a platform to explore a broad spectrum of complex material structures that commonly exist in natural ECMs. Our method to generate semiquantitative maps on the CBC array may facilitate the systematic design of biomaterial micro/nano topographies for direct cell reprogramming. Lastly, our results highlight the importance of considering complex ECM structures in biomaterial design for cell culture and tissue engineering. Specifically, a hierarchical nanopattern screened by our cell mapping platform enhanced the conversion of fibroblasts into mature neurons. Mechanistically, multiscale topographies in the hierarchical nanopattern had cooperative functions in regulating nuclear polarization and epigenetic modulation through cytoskeletal remodeling. Incorporating this multiscale structural design principle and combining it with advanced spatial omics approaches (e.g., spatial transcriptomics) would be important for future development of biomaterials with higher structural complexities and provide an alternative strategy to improve the efficiency of current biomaterials for cell reprogramming and tissue engineering. Moving forward, it would be crucial to understand the scale of forces involved in the reprogramming of fibroblast on the CBC array. Despite current methods for measuring the mechanical forces generated by cells, such as fluorescent tension probe, AFM, and micropillar-based methods, it remains a challenge to apply current methods for monitoring forces involved in thousands of different cell-topography interactions on a large substrate. Also, more detailed characterization and screening of subtype neurons under various array variables, including composition and stiffness of the CBC array (Figures S13 and 14), would highlight the critical role of biophysical cues in regulating diverse neuronal differentiation and reprogramming pathways.

METHODS

Fabrication of Combinatorial Nanoarray Using DIL with Curved Interferometer. A glass slide with 0.5 mm thickness and an active patterning area of 1×1 cm² was sequentially sonicated in 1% Triton X-100 [4-(C_8H_{17}) C_6H_4 OCH₂CH₂·nOH), $n \sim 10$, Sigma-Aldrich], ethanol (95%), and deionized water 20 min, each for cleaning followed drying using N_2 gas. 1 Afterward, the substrate was functionalized with (CH3)₃SiNHSi(CH₃)₃ [hexamethyldisilazane (HMDS), Sigma-Aldrich] via a vapor phase deposition method in a vacuum chamber and then spin-coated (Laurell Technologies, USA) AZ2020 [or AZ1505 when making dot arrays, or polyethylene glycol diacrylate (PEG-DA, molecular weights of 1000, 700, and 500 when making array with stiffnesses of 25 kPa, 332 kPa, and 2 MPa)] a UVcross-linkable photoresist (PR) after 1:0.8 dilution with an AZ EBR solvent (Microchemicals, Germany). After soft baking at 120 °C for the 60 s (PEG-DA does not require baking processes), the PR-coated glass was exposed to interferometry coupled with a UV laser (He-Cd 325 nm laser, KIMMON KOHA Laser Systems, Japan) at the wavelength of 325 nm and a power density of 0.8 mW/cm². The generation of differentially structured combinatorial nanoarrays is achieved by modulating the parameters of unsymmetrical (convexshaped) Lloyd's mirror interferometer (focal length of 15 mm) guided by our optical simulations. Line-shaped combinatorial nanoarrays are

formed via a single exposure, while the grid or dot-shaped combinatorial nanoarrays are formed through two exposure events. The angles in the grid-shaped combinatorial nanoarrays can be controlled by the rotation angle between two exposure events, which is 90° if not mentioned and 120° when the 120° grid pattern is desired. As controls, regular Lloyd's mirror (flat shaped) was integrated into the interferometer to create homogeneous PR patterns with single topographies. After the exposure, PR-coated substrates were baked at 120 °C for 1 min (positive PR of AZ1505 does not require a postbaking step) and then etched by the developer solvent. Typically, a hologram appears when the uncross-linked PR is removed by the developer (the PEG-DA array does not require the developing step).

Characterization of Combinatorial Nanoarrays. To characterize combinatorial nanoarrays at different scales, we performed optical (phase image collected by a T2500 inverted fluorescence microscope), field-emission scanning electron microscope (Zeiss 982, 20 kV), helium-ion microscopy (HIM, Carl Zeiss, Orion Plus) and AFM (Park Systems, NX10 series) on the combinatorial nanoarrays. In the AFM experiment, tapping mode was used and XYZ positioning is controlled by piezoelectric scanners.

Cell Culture. BJ or human dermal fibroblast cell line was purchased from ATCC and harvested from the foreskin of a newborn male human. Passages 4–7 were used throughout the experiments. 20% FBS with DMEM as the basal media was used to maintain and expand the cell line. We formulated the neuronal reprogramming media as follows: B27, N2, Glutamax, bFGF (100 ng/mL), ISX9 (20 μ M), Forskolin (100 μ M), Chir99021 (20 μ M), and dCAMP (100 ng/mL) with basal media composed of neurobasal and DMEM/F12 media at a 1:1 ratio, which is adapted from a small molecule-based transdifferentiation protocol of murine fibroblasts but without epigenetic modulators. Prior to the neuronal reprogramming, substrates containing combinatorial nanoarrays and other structures were coated with Matrigel (Corning) 1:200 dilution.

Antibodies and Immunostaining (Table S1). We conducted immunocytochemistry to study topography-regulated cell behaviors after fixation on the combinatorial nanoarrays. All fluorescence images were obtained using a Nikon T2500 inverted fluorescence microscope. The nucleus was stained with DAPI (1:500 dilution, Life Technologies) for 30 min and then washed with PBS three times. Cells were permeabilized with 0.1% Triton X-100 in PBS for 10 min, and nonspecific binding was blocked with 5% normal goat serum (NGS, Life Technologies) in DPBS for 1 h at room temperature. In the differentiation and axonal growth assay, cells were stained with neuronal markers TuJ1 and MAP2 using the mouse monoclonal antibody against TuJ1 (1:200 dilution, Biolegend) and MAP2 (1:300 dilution, Cell Signaling). After incubating overnight at 4 °C in a solution of these antibodies in PBS containing 10% NGS, and washing three times with PBS, the samples were incubated for 1 h at room temperature in a solution of antimouse secondary antibody labeled with Alexa Flour 568 (1:100, Life Technologies) in PBS containing 10% NGS and washed with DPBS three times thereafter. In the adhesion assay, cells were stained with TRITC-labeled Phalloidin (1:100 dilution, ThermoFisher) and DAPI (1:500 dilution, Life Technologies) for 1 h, followed by DPBS washing.

Fabrication of Hierarchical Structures Using Photomask-LIL Combined Hierarchical Lithography (Hierarchical Nanolithography, Table S3). Glass substrates were cleaned and coated with AZ2020 PR using identical procedures followed by soft baking at 120 °C for 60 s. After placing the PR-coated substrates onto the sample holder vertical to the regularly shaped (flat) Lloyd's mirror, a chrome mask with designated line shapes was fixed on top of the substrates via vacuum forces. The direction of line masks was adjusted to be vertical to the interferometric events. Afterward, the PR underwent the LIL procedure via a 20 s exposure followed by postbaking and developing.

Statistical Analysis. Data are presented as mean ± standard deviation of the mean unless indicated otherwise. One-way ANOVA with Tukey posthoc analysis was used for all the multigroup comparisons. Sample number was labeled in the figure caption of each figure. When the sample number was over 10, individual data

points were plotted in the bar graphs. Graphs plotting and statistical analysis were performed using OriginLab or Excel.

ASSOCIATED CONTENT

Supporting Information

The Supporting Information is available free of charge at https://pubs.acs.org/doi/10.1021/acsnano.1c10344.

Methods for DIL, substrate fabrication, CBC array characterization, cellular reprogramming, immunostaining, cell imaging and mapping, data analysis, and gene analysis. Figures illustrating the high complexity of natural and synthetic ECM seen in the literature, data for showing the formation of homogeneous nanoarrays with single structures generated by laser interference lithography, laser setup for DIL and calculations of the pattern pitches, optical simulation for predicting the optical pathways in DIL, nondirected cell migration on the combinatorial nanoarray, fabrication of combinatorial nanoarrays at higher complexities, modulation of composition, mechanical and biochemical properties of combinatorial nanoarrays, fabrication of homogeneous hierarchical nanostructures by developing hierarchical lithography, and characterization of cytoskeletal remodeling of fibroblasts on different ECM nanostructures (PDF)

AUTHOR INFORMATION

Corresponding Author

Ki-Bum Lee — Department of Chemistry and Chemical Biology, Rutgers University, the State University of New Jersey, Piscataway, New Jersey 08854, United States; orcid.org/0000-0002-8164-0047; Email: kblee@rutgers.edu

Authors

Letao Yang — Department of Chemistry and Chemical Biology, Rutgers University, the State University of New Jersey, Piscataway, New Jersey 08854, United States; orcid.org/ 0000-0002-0572-9787

Brian M. Conley – Department of Chemistry and Chemical Biology, Rutgers University, the State University of New Jersey, Piscataway, New Jersey 08854, United States

Christopher Rathnam — Department of Chemistry and Chemical Biology, Rutgers University, the State University of New Jersey, Piscataway, New Jersey 08854, United States; orcid.org/0000-0003-3111-4687

Hyeon-Yeol Cho – Department of Chemistry and Chemical Biology, Rutgers University, the State University of New Jersey, Piscataway, New Jersey 08854, United States; orcid.org/0000-0003-1897-1166

Thanapat Pongkulapa — Department of Chemistry and Chemical Biology, Rutgers University, the State University of New Jersey, Piscataway, New Jersey 08854, United States; orcid.org/0000-0003-0678-1736

Brandon Conklin — Department of Chemistry and Chemical Biology, Rutgers University, the State University of New Jersey, Piscataway, New Jersey 08854, United States;
ocid.org/0000-0002-6834-3275

Complete contact information is available at: https://pubs.acs.org/10.1021/acsnano.1c10344

Notes

The authors declare no competing financial interest.

ACKNOWLEDGMENTS

K.-B.L. gratefully acknowledges the partial financial support from the NSF (CBET-1803517), the New Jersey Commission on Spinal Cord (CSCR17IRG010; CSCR16ERG019), NIH R21 (R21AR071101), and NIH R01 (1R01DC016612, 3R01DC016612-01S1, 3R01DC016612-04S2, 3R01DC016612-04S1, 5R01DC016612-02S1), NJ Health Foundation, Grossman Innovation Prize, and NJ ACTS-Pilot Project grant. The authors acknowledge Prof. Jin-Ho Lee, Dr. Jin-Ho Yoon, Yannan Hou, and Shenqiang Wang for their generous help with substrate fabrication and characterization.

REFERENCES

- (1) de la Torre, D.; Chin, J. W. Reprogramming The Genetic Code. *Nat. Rev. Genet.* **2021**, 22, 169–184.
- (2) Shakiba, N.; Fahmy, A.; Jayakumaran, G.; mcgibbon, S.; David, L.; Trcka, D.; Elbaz, J.; Puri, M. C.; Nagy, A.; van der Kooy, D.; Goyal, S.; Wrana, J. L.; Zandstra, P. W. Cell Competition During Reprogramming Gives Rise To Dominant Clones. *Science* **2019**, *364*, 354
- (3) Hussey, G. S.; Dziki, J. L.; Badylak, S. F. Extracellular Matrix-Based Materials For Regenerative Medicine. *Nat. Rev. Mater.* **2018**, 3, 159–173.
- (4) Tsunemoto, R.; Lee, S.; Sztics, A.; Chubukov, P.; Sokolova, I.; Blanchard, J. W.; Eade, K. T.; Bruggemann, J.; Wu, C. L.; Torkamani, A.; Sanna, P. P.; Baldwin, K. K. Diverse Reprogramming Codes For Neuronal Identity. *Nature* **2018**, *557*, 375–380.
- (5) Kim, D.; Arai, Y.; Lee, Y.; Choi, B.; Lee, S. Regulation of Cell reprogramming in 3D Microenvironment Interactions. *Tissue Eng. Part A* **2017**, 23, S151.
- (6) Murphy, W. L.; mcdevitt, T. C.; Engler, A. J. Materials As Stem Cell Regulators. *Nat. Mater.* **2014**, *13*, 547–557.
- (7) Hansel, C. S.; Crowder, S. W.; Cooper, S.; Gopal, S.; João Pardelha da Cruz, M.; de Oliveira Martins, L.; Keller, D.; Rothery, S.; Becce, M.; Cass, A. E. G.; Bakal, C.; Chiappini, C.; Stevens, M. M. Nanoneedle-Mediated Stimulation of Cell Mechanotransduction Machinery. ACS Nano 2019, 13, 2913–2926.
- (8) Engler, A. J.; Sen, S.; Sweeney, H. L.; Discher, D. E. Matrix Elasticity Directs Stem Cell Lineage Specification. *Cell* **2006**, *126*, 677–689.
- (9) Downing, T. L.; Soto, J.; Morez, C.; Houssin, T.; Fritz, A.; Yuan, F.; Chu, J.; Patel, S.; Schaffer, D. V.; Li, S. Biophysical Regulation of Epigenetic State And Cell Reprogramming. *Nat. Mater.* **2013**, *12*, 1154–1162
- (10) Jin, Y.; Lee, J. S.; Kim, J.; Min, S.; Wi, S.; Yu, J. H.; Chang, G. E.; Cho, A. N.; Choi, Y.; Ahn, D. H.; Cho, S. R.; Cheong, E.; Kim, Y. G.; Kim, H. P.; Kim, Y.; Kim, D. S.; Kim, H. W.; Quan, Z.; Kang, H. C.; Cho, S. W. Three-Dimensional Brain-Like Microenvironments Facilitate The Direct Reprogramming Of Fibroblasts Into Therapeutic Neurons. *Nat. Biomed. Eng.* **2018**, *2*, 522–539.
- (11) Meng, X.; Zhou, A.; Huang, Y.; Zhang, Y.; Xu, Y.; Shao, K.; Ning, X. N-Cadherin Nanoantagonist Driven Mesenchymal-to-Epithelial Transition in Fibroblasts for Improving Reprogramming Efficiency. *Nano Lett.* **2021**, *21*, 5540–5546.
- (12) Nemec, S.; Kilian, K. A. Materials Control Of The Epigenetics Underlying Cell Plasticity. *Nat. Rev. Mater.* **2021**, *6*, 69–83.
- (13) Wang, Y.; Wang, Z.; Xie, K.; Zhao, X.; Jiang, X.; Chen, B.; Han, Y.; Lu, Y.; Huang, L.; Zhang, W.; Yang, Y.; Shi, P. High-Efficiency Cell reprogramming by Nanoscale Puncturing. *Nano Lett.* **2020**, *20*, 5473–5481.
- (14) Place, E. S.; Evans, N. D.; Stevens, M. M. Complexity in Biomaterials For Tissue Engineering. *Nat. Mater.* **2009**, *8*, 457–470. (15) Darnell, M.; Mooney, D. J. Leveraging Advances In Biology To Design Biomaterials. *Nat. Mater.* **2017**, *16*, 1178–1185.

- (16) Unadkat, H. V.; Hulsman, M.; Cornelissen, K.; Papenburg, B. J.; Truckenmuller, R. K.; Carpenter, A. E.; Wessling, M.; Post, G. F.; Uetz, M.; Reinders, M. J. T.; Stamatialis, D.; van Blitterswijk, C. A.; de Boer, J. An Algorithm-Based Topographical Biomaterials Library To Instruct Cell Fate. *Proc. Natl. Acad. Sci. U.S.A.* **2011**, *108*, 16565–16570.
- (17) von Erlach, T. C.; Bertazzo, S.; Wozniak, M. A.; Horejs, C. M.; Maynard, S. A.; Attwood, S.; Robinson, B. K.; Autefage, H.; Kallepitis, C.; Hernandez, A. D.; Chen, C. S.; Goldoni, S.; Stevens, M. M. Cell-Geometry-Dependent Changes In Plasma Membrane Order Direct Stem Cell Signalling And Fate. *Nat. Mater.* **2018**, *17*, 237–242.
- (18) Xue, X.; Sun, Y.; Resto-Irizarry, A. M.; Yuan, Y.; Aw Yong, K. M.; Zheng, Y.; Weng, S.; Shao, Y.; Chai, Y.; Studer, L.; Fu, J. Mechanics-Guided Embryonic Patterning Of Neuroectoderm Tissue From Human Pluripotent Stem Cells. *Nat. Mater.* **2018**, *17*, 633–641.
- (19) Yim, E. K. F.; Darling, E. M.; Kulangara, K.; Guilak, F.; Leong, K. W. Nanotopography-Induced Changes In Focal Adhesions, Cytoskeletal Organization, And Mechanical Properties Of Human Mesenchymal Stem Cells. *Biomaterials* **2010**, *31*, 1299–1306.
- (20) Seo, J.; Shin, J.-Y.; Leijten, J.; Jeon, O.; Camci-Unal, G.; Dikina, A. D.; Brinegar, K.; Ghaemmaghami, A. M.; Alsberg, E.; Khademhosseini, A. High-Throughput Approaches For Screening And Analysis Of Cell Behaviors. *Biomaterials* **2018**, *153*, 85–101.
- (21) Gobaa, S.; Hoehnel, S.; Roccio, M.; Negro, A.; Kobel, S.; Lutolf, M. P. Artificial Niche Microarrays For Probing Single Stem Cell Fate In High Throughput. *Nat. Meth.* **2011**, *8*, 949–955.
- (22) Vega, S. L.; Kwon, M. Y.; Song, K. H.; Wang, C.; Mauck, R. L.; Han, L.; Burdick, J. A. Combinatorial Hydrogels With Biochemical Gradients For Screening 3D Cellular Microenvironments. *Nat. Commun.* **2018**, *9*, 614.
- (23) Baek, S.; Quan, X.; Kim, S.; Lengner, C.; Park, J.-K.; Kim, J. Electromagnetic Fields Mediate Efficient Cell reprogramming into a Pluripotent State. *ACS Nano* **2014**, *8*, 10125–10138.
- (24) Amamoto, R.; Arlotta, P. Development-Inspired Reprogramming of the Mammalian Central Nervous System. *Science* **2014**, *343*, 1239882.
- (25) Tran, T. T.; Wang, D.; Xu, Z.-Q.; Yang, A.; Toth, M.; Odom, T. W.; Aharonovich, I. Deterministic Coupling of Quantum Emitters in 2D Materials to Plasmonic Nanocavity Arrays. *Nano Lett.* **2017**, *17*, 2634–2639.
- (26) Min, S.; Li, S.; Zhu, Z.; Liu, Y.; Liang, C.; Cai, J.; Han, F.; Li, Y.; Cai, W.; Cheng, X.; Li, W.-D. Ultrasensitive Molecular Detection by Imaging of Centimeter-Scale Metasurfaces with a Deterministic Gradient Geometry. *Adv. Mater.* **2021**, *33*, 2100270.
- (27) Kim, H.; Jung, H.; Lee, D.-H.; Lee, K. B.; Jeon, H. Period-Chirped Gratings Fabricated By Laser Interference Lithography With a Concave Lloyd Mirror. *Appl. Opt.* **2016**, *55*, 354–359.
- (28) Lasagni, A. F. Laser Interference Patterning Methods: Possibilities For High-Throughput Fabrication Of Periodic Surface Patterns. *Adv. Opt. Technol.* **2017**, *6*, 265–275.
- (29) Rossetti, L.; Kuntz, L. A.; Kunold, E.; Schock, J.; Müller, K. W.; Grabmayr, H.; Stolberg-Stolberg, J.; Pfeiffer, F.; Sieber, S. A.; Burgkart, R.; Bausch, A. R. The Microstructure And Micromechanics Of The Tendon-Bone Insertion. *Nat. Mater.* **2017**, *16*, 664–670.
- (30) Mouw, J. K.; Ou, G.; Weaver, V. M. Extracellular Matrix Assembly: A Multi-Scale Deconstruction. *Nat. Rev. Mol. Cell Biol.* **2014**, *15*, 771–785.
- (31) Jin, H.-E.; Jang, J.; Chung, J.; Lee, H. J.; Wang, E.; Lee, S.-W.; Chung, W.-J. Biomimetic Self-Templated Hierarchical Structures of Collagen-Like Peptide Amphiphiles. *Nano Lett.* **2015**, *15*, 7138–7145.
- (32) Ermis, M.; Antmen, E.; Hasirci, V. Micro and Nanofabrication Methods To Control Cell-Substrate Interactions And Cell Behavior: A Review From The Tissue Engineering Perspective. *Bioact. Mater.* **2018**, *3*, 355–369.
- (33) Wang, P. Y.; Clements, L. R.; Thissen, H.; Jane, A.; Tsai, W. B.; Voelcker, N. H. Screening Mesenchymal Stem Cell Attachment And Differentiation On Porous Silicon Gradients. *Adv. Funct. Mater.* **2012**, 22, 3414–3423.

- (34) Yang, M. T.; Fu, J.; Wang, Y.-K.; Desai, R. A.; Chen, C. S. Assaying stem cell mechanobiology on microfabricated elastomeric substrates with geometrically modulated rigidity. *Nat. Protoc.* **2011**, *6*, 187–213.
- (35) Liu, Y.; Galior, K.; Ma, V. P.-Y.; Salaita, K. Molecular tension probes for imaging forces at the cell surface. *Acc. Chem. Res.* **2017**, *50*, 2915–2924.
- (36) Park, J.; Kim, D.-H.; Kim, H.-N.; Wang, C. J.; Kwak, M. K.; Hur, E.; Suh, K.-Y.; An, S. S.; Levchenko, A. Directed Migration Of Cancer Cells Guided By The Graded Texture Of The Underlying Matrix. *Nat. Mater.* **2016**, *15*, 792–801.
- (37) Treutlein, B.; Lee, Q. Y.; Camp, J. G.; Mall, M.; Koh, W.; Shariati, S. A. M.; Sim, S.; Neff, N. F.; Skotheim, J. M.; Wernig, M.; Quake, S. R. Dissecting Direct Reprogramming From Fibroblast To Neuron Using Single-Cell RNA-Seq. *Nature* **2016**, *534*, 391–395.
- (38) Lee, Y. S.; Jung, W. Y.; Heo, H.; Park, M. G.; Oh, S.-H.; Park, B.-G.; Kim, S. Exosome-Mediated Ultra-Effective Direct Conversion of Human Fibroblasts into Neural Progenitor-like Cells. *ACS Nano* **2018**, *12*, 2531–2538.
- (39) Krishnakumar, R.; Blelloch, R. H. Epigenetics of Cell Reprogramming. Curr. Opin. Genet. & Devel. 2013, 23, 548–555.
- (40) Nie, B.; Wang, H.; Laurent, T.; Ding, S. Cell Reprogramming: A Small Molecule Perspective. *Curr. Opin. Cell Bio.* **2012**, 24, 784–792.
- (41) Gong, L.; Cao, L.; Shen, Z.; Shao, L.; Gao, S.; Zhang, C.; Lu, J.; Li, W. Materials for Neural Differentiation, Trans-Differentiation, and Modeling of Neurological Disease. *Adv. Mater.* **2018**, *30*, 1705684.
- (42) Lee, Y. S.; Jung, W. Y.; Heo, H.; Park, M. G.; Oh, S.-H.; Park, B.-G.; Kim, S. Exosome-Mediated Ultra-Effective Direct Conversion of Human Fibroblasts into Neural Progenitor-like Cells. *ACS Nano* **2018**, *12*, 2531–2538.
- (43) Mattiassi, S.; Rizwan, M.; Grigsby, C. L.; Zaw, A. M.; Leong, K. W.; Yim, E. K. Enhanced Efficiency Of Nonviral Direct Neuronal Reprogramming On Topographical Patterns. *Biomaterials Science* **2021**, *9*, 5175–5191.
- (44) Hong, H.; Min, S.; Koo, S.; Lee, Y.; Yoon, J.; Jang, W. Y.; Kang, N.; Thangam, R.; Choi, H.; Jung, H. J.; Han, S.-B.; Wei, Q.; Yu, S.-H.; Kim, D.-H.; Paulmurugan, R.; Jeong, W. K.; Lee, K.-B.; Hyeon, T.; Kim, D.; Kang, H. Dynamic Ligand Screening by Magnetic Nanoassembly Modulates Stem Cell Differentiation. *Adv. Mater.* 2022, 34, 2105460.
- (45) Nie, B.; Wang, H.; Laurent, T.; Ding, S. Cellular Reprogramming: A Small Molecule Perspective. *Curr. Opin. Cell Biol.* **2012**, *24*, 784–792.
- (46) Cao, C.; Chan, H. F.; Zang, J.; Leong, K. W.; Zhao, X. Harnessing Localized Ridges for High-Aspect-Ratio Hierarchical Patterns with Dynamic Tunability and Multifunctionality. *Adv. Mater.* **2014**, *26*, 1763–1770.
- (47) Onses, M. S.; Song, C.; Williamson, L.; Sutanto, E.; Ferreira, P. M.; Alleyne, A. G.; Nealey, P. F.; Ahn, H.; Rogers, J. A. Hierarchical Patterns Of Three-Dimensional Block-Copolymer Films Formed By Electrohydrodynamic Jet Printing And Self-Assembly. *Nat. Nanotechnol.* **2013**, *8*, 667–675.
- (48) Henzie, J.; Lee, M. H.; Odom, T. W. Multi-scale Patterning Of Plasmonic Metamaterials. *Nat. Nanotechnol.* **2007**, *2*, 549–554.
- (49) Maurer, M.; Lammerding, J. The Driving Force: Nuclear Mechanotransduction in Cellular Function, Fate, and Disease. *Annu. Rev. Biomed. Eng.* **2019**, *21*, 443–468.
- (50) Yoo, J.; Noh, M.; Kim, H.; Jeon, N. L.; Kim, B.-S.; Kim, J. Nanogrooved Substrate Promotes Direct Lineage Reprogramming Of Fibroblasts To Functional Induced Dopaminergic Neurons. *Biomaterials* **2015**, *45*, 36–45.
- (51) Dalby, M. J.; Gadegaard, N.; Oreffo, R. O. Harnessing Nanotopography And Integrin-Matrix Interactions To Influence Stem Cell Fate. *Nat. Mater.* **2014**, *13*, 558–569.
- (52) Zhang, W.; Wang, G.; Liu, Y.; Zhao, X.; Zou, D.; Zhu, C.; Jin, Y.; Huang, Q.; Sun, J.; Liu, X.; Jiang, X.; Zreiqat, H. The Synergistic Effect Of Hierarchical Micro/Nano-Topography And Bioactive Ions For Enhanced Osseointegration. *Biomaterials* **2013**, *34*, 3184–3195.

- (53) Zhang, M.; Lin, Y.-H.; Sun, Y. J.; Zhu, S.; Zheng, J.; Liu, K.; Cao, N.; Li, K.; Huang, Y.; Ding, S. Pharmacological Reprogramming of Fibroblasts into Neural Stem Cells by Signaling-Directed Transcriptional Activation. *Cell Stem Cell* **2016**, *18*, 653–667.
- (54) Li, X.; Zuo, X.; Jing, J.; Ma, Y.; Wang, J.; Liu, D.; Zhu, J.; Du, X.; Xiong, L.; Du, Y.; et al. Small-Molecule-Driven Direct Reprogramming Of Mouse Fibroblasts Into Functional Neurons. *Cell stem cell* **2015**, *17*, 195–203.

□ Recommended by ACS

Nanoscale Surface Topography Reduces Focal Adhesions and Cell Stiffness by Enhancing Integrin Endocytosis

Xiao Li, Bianxiao Cui, et al.

AUGUST 04, 2021 NANO LETTERS

Suspendable Hydrogel Nanovials for Massively Parallel Single-Cell Functional Analysis and Sorting

Joseph de Rutte, Dino Di Carlo, et al.

MARCH 24, 2022

ACS NANO

READ 🗹

Tuning the Nanotopography and Chemical Functionality of 3D Printed Scaffolds through Cellulose Nanocrystal Coatings

Mouhanad Babi, Jose Moran-Mirabal, et al.

NOVEMBER 17, 2021

ACS APPLIED BIO MATERIALS

READ **C**

DNA Tension Probes Show that Cardiomyocyte Maturation Is Sensitive to the Piconewton Traction Forces Transmitted by Integrins

Sk Aysha Rashid, Khalid Salaita, et al.

MARCH 24, 2022

ACS NANO

READ 🗹

Get More Suggestions >